Itinerant ferromagnetism in the periodic Anderson model

C. D. Batista,[1] J. Bonča,[2] and J. E. Gubernatis[1]
[1]*Center for Nonlinear Studies and Theoretical Division, Los Alamos National Laboratory, Los Alamos, New Mexico 87545, USA*
[2]*Department of Physics, FMF, University of Ljubljana and J. Stefan Institute, Ljubljana, Slovenia*
(Received 10 March 2003; revised manuscript received 8 October 2003; published 29 December 2003)

We introduce a mechanism for itinerant ferromagnetism, based on a simple two-band model. The model includes an uncorrelated and dispersive band hybridized with a second band which is narrow and correlated. The simplest Hamiltonian containing these ingredients is the periodic Anderson model (PAM). Using quantum Monte Carlo and analytical methods, we show that the PAM and an extension of it contain the mechanism and exhibit a nonsaturated ferromagnetic ground state in the intermediate-valence regime. We propose that the mechanism, which does not assume an intra-atomic Hund's coupling, is present in both the iron group and in some *f* electron compounds like $Ce(Rh_{1-x}Ru_x)_3B_2$, $La_xCe_{1-x}Rh_3B_2$, and the uranium monochalcogenides US, USe, and UTe.

DOI: 10.1103/PhysRevB.68.214430 PACS number(s): 75.10.Lp

I. INTRODUCTION

This work is an extension of a previous letter[1] where we have described the basic ideas. Here we introduce a different mechanism for itinerant ferromagnetism, which is based on a simple two-band model. We show that the mechanism is supported by the numerical results obtained from quantum Monte Carlo (QMC) simulations of the periodic Anderson model (PAM). We also analyze the experimental consequences for some *f* electron compounds and the iron group. However, before describing the details of our mechanism, it is useful to develop a historical perspective on itinerant ferromagnetism.

The first attempt at analyzing a real FM metal, like Ni, was made by Slater.[2] He concluded that the main contribution to the exchange energy is provided by intra-atomic interactions. In the meantime, Stoner[3] introduced his picture where the metallic ferromagnetism results from holes in the $3d$ band interacting via an exchange energy proportional to the relative magnetization and obeying Fermi-Dirac statistics. However, the model considered first by Stoner[3] and later by Wohlfarth[4] did not take into account the correlations of the $3d$ electrons, except for the constraints imposed by the Pauli exclusion principle. In other words, they did not consider the fact that the Coulomb repulsion tends to keep the electrons apart.

In 1953, the importance of these correlations was pointed out by van Vleck.[5] He emphasized that the energy required to tear off an electron increases rapidly with the degree of ionization. (The energy of two Ni atoms in a $3d^9$ configuration is appreciably lower than having one atom in the $3d^8$ state and the other one in $3d^{10}$.) Based on this observation, he proposed an alternative picture (minimum polarity model) where the states of higher ionization in Ni are ruled out completely, and the configuration $3d^{9.4}$ is considered to be 40% $3d^{10}$ and 60% percent $3d^9$. The lattice sites occupied by $3d^9$ and $3d^{10}$ configurations are continuously redistributing in his picture. The van Vleck proposal is the precursor of the Hubbard model for infinite *U*.

Following Slater,[6] van Vleck[5] speculated that the contamination by states of higher polarity, not included in his model, provides the exchange interaction (intra-atomic in this case) necessary for ferromagnetism. Hence he calculated the effective nearest-neighbor magnetic interaction induced by second-order perturbative fluctuations from the d^9+d^9 configuration to the d^8+d^{10}. In this way, van Vleck arrived at a model which describes itinerant and correlated (only allowing d^9 and d^{10} configurations) holes with a nearest-neighbor exchange interaction $\alpha \mathbf{S_i}\cdot\mathbf{S_j}$ (generalized Heisenberg model). However, as van Vleck explained at the end of his paper,[5] the sign and the magnitude of α are very sensitive to the precise values of the energies of the different possible intermediate states (singlets or triplets) in the d^8 configuration.

In 1963, the one-band Hubbard model was proposed independently by Gutzwiller,[7] Hubbard,[8] and Kanamori[9] to explain the metallic ferromagnetism in the $3d$ transition metals. The Hubbard model incorporates the kinetic energy in a *single nondegenerate band* with an intra-atomic Coulomb repulsion *U* to describe the electrons in the *s* band of the transition metals. In contrast to the previous models, the Hubbard model does not include any explicit exchange interaction which favors a ferromagnetic phase. The implicit question raised by this proposal is: Can ferromagnetism emerge from the interplay between the kinetic energy and the Coulomb repulsion, or it is strictly necessary to include an explicit exchange interaction provided by the intra-atomic Hund's coupling? This simple question becomes even more relevant if we consider *f*-electron itinerant ferromagnets, like $CeRh_3B_2$,[10] whose only local magnetic coupling is antiferromagnetic.

Unfortunately, with the exception of Nagaoka's[11] and Lieb's[12,13] theorems, the subsequent theoretical approaches were not controlled enough to determine whether the Hubbard model has a ferromagnetic (FM) phase. The central issue is the precise evaluation of the energy for the paramagnetic (PM) phase. Because it does not properly incorporate the correlations, mean-field theory overestimates this energy and predicts a large FM region.[14] In contrast, numerical calculations have narrowed the extent of this phase to a small region around the Nagaoka point.[11,15]

Going beyond the simple one-band Hubbard model has

been advocated, for instance, by Vollhardt *et al.*[14] They note that the inclusion of additional Coulomb density-density interactions, correlated hoppings, and direct exchange interactions favors FM ordering in the single-band Hubbard model. In fact, a very simple analysis shows that increasing the density of states $\mathcal{D}(E)$ below the Fermi energy E_F and placing E_F close to the lower band edge increases the FM tendency. One can achieve this by including a next-nearest-neighbor hopping t' or by placing the hoppings on frustrated (nonbipartite) lattices. The effectiveness of t' was studied numerically by Hlubina *et al.*[16] for the Hubbard model on a square lattice. They found a FM state when the van Hove singularity in $\mathcal{D}(E)$ occurred at E_F. However, this phase was not robust against very small changes in t'.

While the Hubbard model is so reluctant to have a FM state, there is an increasing amount of evidence indicating that the periodic Anderson model (PAM) has a FM phase in a large region of its quantum phase diagram.[1,17–30] Since the *d* orbitals of the transition metals are hybridized with the $s-p$ bands, we can consider the inclusion of a second band as the next step in the search of itinerant ferromagnetism from pure Coulomb repulsions.

Ferromagnetism is readily found in the PAM by various mean-field approximations in any dimension. For example, using a slave-boson mean-field theory (SBMFT) for the symmetric PAM, Möller and Wölfe[21] found a PM or antiferromagnetic (AF) phase at half filling depending on the value of the Coulomb repulsion *U*. More recently, the SBMFT calculations of Doradziński and Spalek[22,23] found wide regions of ferromagnetism in the intermediate valence regime that surprisingly extended well below 1/4 filling.

As another example, a ferromagnetic phase is also obtained when the dynamical mean-field theory (DMFT) (Refs. 31–34) is applied to the PAM.[24–30] Tahvildar-Zadeh *et al.* found a region of ferromagnetism and studied its temperature dependence. At very low temperatures, their ferromagnetic region extended over a wide range of electron fillings and in many cases embraced the electron filling of 3/8. More recently Meyer and Nolting[28–30] appended perturbation theory to DMFT and also predicted ferromagnetism over a broad range of electron filling extending below 1/4 filling. In addition, Schwieger and Nolting[35] also considered an extension of the PAM, similar to the one considered here, to estimate the importance of $s-d$ hybridization for the magnetic properties of transition metals.

There is also a considerable amount of numerical evidence showing ferromagnetic solutions for the ground state of the PAM. Noack and Guerrero,[19] for example, found partially and completely saturated ferromagnetism using the density-matrix renormalization-group (DMRG) method in one dimension. They considered a parameter regime where there is one electron in each *f* orbital. For a sufficiently large value of *U*, the model exhibited a ferromagnetic ground state. Beyond an interaction-dependent value of the doping and a doping-dependent value of *U*, this state disappeared. The ferromagnetic phase was a peninsula in a phase diagram that was otherwise a sea of paramagnetism except at 1/4 and 1/2 filling where the ground state of the PAM was antiferromagnetic.

Our previous[17] and new QMC results qualitatively agree with the DMRG work; however, the phases we find quantitatively and qualitatively disagree with those derived from the mean-field approximations. Quantitatively, we find ferromagnetism in a narrower doping range than the one predicted by the DMFT and SBMFT calculations. For fillings between 3/8 and 1/2, QMC predicts a PM region, whereas mean-field theory predicts ferromagnetic states in part of that region. In fact, at a filling of 3/8 where DMFT calculations predict ferromagnetism, we find a spin-density-wave state with a wave vector equal to $(\pi,0)$ or $(0,\pi)$.

The mechanism we introduce in the present paper operates when the system is in a mixed-valence regime. This regime has been studied numerically only in the context of DMFT.[28] We will show, however, that the ferromagnetic solution obtained with DMFT in the mixed-valence regime has a different origin and therefore is not representative of our mechanism. The main ingredient for our mechanism is an uncorrelated dispersive band which is hybridized with a correlated and narrow band. We show that the PAM supports our mechanism by doing quantum Monte Carlo (QMC) simulations on one- and two-dimensional lattices. The results of these simulations are interpreted with an effective Hamiltonian derived from the PAM. In this way, we establish that the mechanism can be interpreted as a generalization to the lattice of the first Hund's rule for the atom. The two level band structure generated by the hybridization gap recreates, for the lattice, the shell-like level structure of the hydrogenic atom. When the lower shell is incomplete, the local part of the Coulomb interaction is minimized by polarizing the electrons which are occupying the incomplete shell.

II. MODEL

The PAM was originally introduced to explain the properties of the rare-earth and actinide metallic compounds including the so called heavy fermion compounds. A very simple extension of this model can also be applied to the description of many transition metals.[35,36] The basic ingredients of this model are a narrow and correlated *a* band hybridized with a despersive and uncorrelated *b* band. The Hamiltonian associated with this model is

$$H = H_0 + H_U$$

$$\begin{aligned} H_0 = & -t_a \sum_{\langle \mathbf{r},\mathbf{r}'\rangle,\sigma} (a^\dagger_{\mathbf{r}\sigma} a_{\mathbf{r}'\sigma} + a^\dagger_{\mathbf{r}'\sigma} a_{\mathbf{r}\sigma}) + \epsilon_a \sum_{\mathbf{r},\sigma} n^a_{\mathbf{r}\sigma} \\ & - t_b \sum_{\langle \mathbf{r},\mathbf{r}'\rangle,\sigma} (b^\dagger_{\mathbf{r}\sigma} b_{\mathbf{r}'\sigma} + b^\dagger_{\mathbf{r}'\sigma} b_{\mathbf{r}\sigma}) \\ & + V \sum_{\mathbf{r},\sigma} (b^\dagger_{\mathbf{r}\sigma} a_{\mathbf{r}\sigma} + a^\dagger_{\mathbf{r}\sigma} b_{\mathbf{r}\sigma}), \end{aligned}$$

$$H_U = \frac{U}{2} \sum_{\mathbf{r},\sigma} n^a_{\mathbf{r}\sigma} n^{a}_{\mathbf{r}\bar{\sigma}}, \tag{1}$$

where $b^\dagger_{\mathbf{r}\sigma}$ and $a^\dagger_{\mathbf{r}\sigma}$ create an electron with spin σ in *b* and *a* orbitals at lattice site $\mathbf{r}$ and $n^a_{\mathbf{r}\sigma} = a^\dagger_{\mathbf{r}\sigma} a_{\mathbf{r}\sigma}$. The t_b and t_a hop-

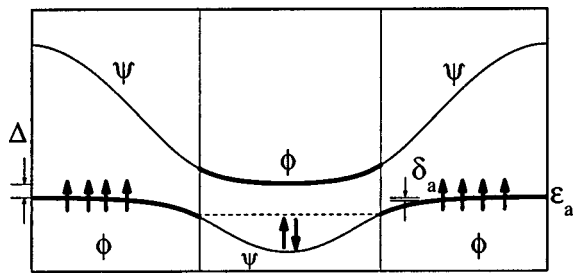

FIG. 1. Illustration of the effective model and the FM mechanism. Δ is the hybridization gap and δ_a is the interval of energy where the electrons are polarized.

pings are only to nearest-neighbor sites. When $t_a=0$, the Hamiltonian is the standard PAM. For the f electron compounds, the a and b orbitals play the role of the f and d orbitals, and $t_a \approx 0$. For transition metals, they correspond to the $3d$ and $4s$ orbitals. Unless otherwise specified, we will set $t_b=1$.

For $U=0$, the resulting Hamiltonian H_0 is easily diagonalized:

$$H_0=\sum_{\mathbf{k},\sigma}\left(E^+_{\mathbf{k}}\beta^\dagger_{\mathbf{k}\sigma}\beta_{\mathbf{k}\sigma}+E^-_{\mathbf{k}}\alpha^\dagger_{\mathbf{k}\sigma}\alpha_{\mathbf{k}\sigma}\right), \tag{2}$$

where the dispersion relations for the upper and the lower bands are

$$E^\pm_{\mathbf{k}}=\frac{1}{2}\left[e^b_{\mathbf{k}}+e^a_{\mathbf{k}}\pm\sqrt{(e^b_{\mathbf{k}}-e^a_{\mathbf{k}})^2+4V^2}\right], \tag{3}$$

with

$$e^b_{\mathbf{k}}=-2t_b\sum_{i=1}^{D}\cos k_{x_i},$$

$$e^a_{\mathbf{k}}=\epsilon_a-2t_a\sum_{i=1}^{D}\cos k_{x_i}, \tag{4}$$

for a hypercubic lattice in dimension D. The operators which create quasiparticles in the lower and upper bands are

$$\alpha^\dagger_{\mathbf{k}\sigma}=u_{\mathbf{k}}a^\dagger_{\mathbf{k}\sigma}+v_{\mathbf{k}}b^\dagger_{\mathbf{k}\sigma},$$

$$\beta^\dagger_{\mathbf{k}\sigma}=-v_{\mathbf{k}}a^\dagger_{\mathbf{k}\sigma}+u_{\mathbf{k}}b^\dagger_{\mathbf{k}\sigma}, \tag{5}$$

with

$$u_{\mathbf{k}}=\frac{E^+_{\mathbf{k}}-e^a_{\mathbf{k}}}{\sqrt{(E^+_{\mathbf{k}}-e^a_{\mathbf{k}})^2+V^2}},$$

$$v_{\mathbf{k}}=\frac{-V}{\sqrt{(E^+_{\mathbf{k}}-e^a_{\mathbf{k}})^2+V^2}}. \tag{6}$$

The noninteracting bands $E^\pm_{\mathbf{k}}$ are plotted in Fig. 1 for a one-dimensional system. If $|V|\ll|t_b|$, we can identify regions with well defined a or b character in the lower and the upper bands. In particular, the case illustrated in Fig. 1 corresponds to a situation where the a and the b bands were crossing before being hybridized ($\epsilon_a>-2t_b$). We see a small region in the center of the lower band which is dispersive and large regions on both sides which are nearly flat. The upper band exhibits the opposite behavior. The nearly flat regions in each band correspond to states with a predominant a character, while the dispersive regions are associated to the states with b character.

III. MECHANISM FOR FERROMAGNETISM

The PAM has different regimes depending on the values of its parameters and the particle concentration $n=N_e/4N$ (N_e is the total number of particles and N is the number of unit cells). If $V\ll|\epsilon_a|$ and $V\ll|U+\epsilon_a|$, there is one particle (magnetic moment) localized in each a orbital, and the fluctuations to the conduction band can be considered in a perturbative way. By this procedure, the PAM can be reduced to the Kondo lattice model (KLM),[37] which contains only one parameter J_K/t with

$$J_K=V^2\sum_{\mathbf{k}}\left[\frac{\Theta(e^b_{\mathbf{k}}-E_F)}{e^b_{\mathbf{k}}-e_a}+\frac{\Theta(E_F-e^b_{\mathbf{k}})}{e_a+U-e^b_{\mathbf{k}}}\right] \tag{7}$$

and $t=t_b$. The KLM has been extensively studied,[38–41] and the evolution of its phase diagram is described for instance in a review article by Tsunetsugu *et al.*[42] One of the earliest approaches to the KLM is the mean-field treatment of Doniach[38] for the related one-dimensional Kondo necklace. For half filling, this approximation leads to a transition from a Néel ordered state in the weak-coupling regime ($J_K\ll|t|$) to a nonmagnetic ''Kondo singlet'' state above the critical value $J^c_K=t$.

Lacroix and Cyrot[43] did a more extensive mean-field treatment for three-dimensional KLM. They also found a magnetically ordered state for weak coupling. In their phase diagram, the ordered state is ferromagnetic for low and intermediate densities of conduction electrons, and antiferromagnetic in the vicinity of half filling. The Kondo singlet phase appears above some critical value of $J^c_K(n)$ in the whole range of concentrations.

Using another mean-field treatment for the one-dimensional KLM, Fazekas and Müller-Hartmann[41] obtained a phase diagram containing only magnetically ordered phases: spiral below some critical value of J_K/t which depends on the particle density and ferromagnetic above this value. To get this result, they fixed the orientation of the localized spins in a spiral ordering and minimized the total energy with respect to the wave vector of the spiral. Even though this treatment of the spin polarized state is valid for classical spins, it neglects completely the Kondo singlet formation which occurs in the strong-coupling limit for the considered case ($S=1/2$).

Sigrist *et al.*[44] gave an exact treatment of one-dimensional KLM for the strong-coupling regime $J_K\gg t$ finding a ferromagnetic phase for any particle density. However, it is important to remark that the mechanism driving the ferromagnetism in the latter case is not the same as the double exchange mechanism associated with the mean-field solution of Fazekas and Müller-Hartmann.[41] To understand this dif-

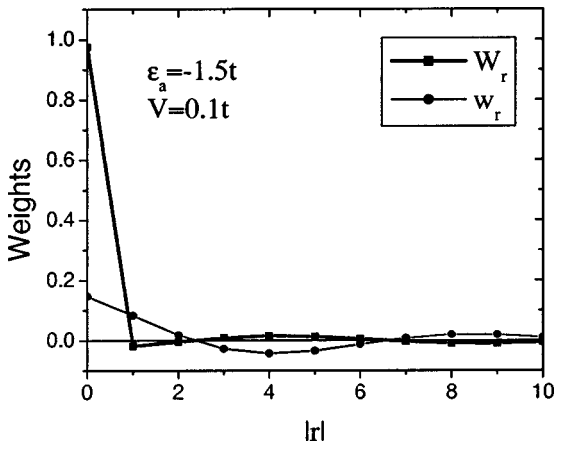

FIG. 2. Weights $W_{\mathbf{r}}$ and $w_{\mathbf{r}}$ as a function of the distance $|\mathbf{r}|$ for a one-dimensional system.

ference, we just need to notice that for $J_K/t=\infty$ mean field[41] predicts a ferromagnetic solution while the exact solution has a complete spin degeneracy. Therefore double exchange is not the mechanism driving the ferromagnetic phase of the KLM (at least when the localized spins are $S=1/2$).

The real mechanism has been unveiled by Sigrist *et al.*[44] who used degenerate perturbation theory to determine the lifting of this degeneracy when the ratio J_K/t becomes finite. The new ground state is an itinerant ferromagnet for any concentration of conduction electrons. In this state, the spins which are not participating in the Kondo singlet are fully polarized. We can see from their solution that the motion of the Kondo singlets stabilizes the FM state in a way similar to the Nagaoka's solution.[11] The second-order effective Hamiltonian obtained after the perturbative calculation includes nearest-neighbor hopping $t/2$, plus a next-nearest-neighbor correlated hopping t' which is order t^2/J_K. Then there are two different ways to move a Kondo singlet from one site to its next-nearest neighbor: by two applications of $t/2$ or by one application of t'. Only when the background is ferromagnetic do both processes lead to the same final state. If t' has the appropriate sign [which is the case for the KLM (Ref. 44)] the resulting interference is ''constructive'' and the FM state has the lowest energy. We can see in this example that the motion of the Kondo singlet can stabilize a magnetic phase.

There are different regimes for which the PAM cannot be reduced to a KLM by a perturbative approach. One of these situations corresponds to the intermediate-valence region: $\epsilon_a \sim E_F$. In this case n_i^a is no longer close to 1 and the a electrons can move. In a recent paper,[45] we have demonstrated that the ground state of the one-dimensional PAM is ferromagnetic when the mixed-valence regime is induced by a strong hybridization ($|V| \gg |t_a|, |t_b|$), U is infinite, and $1/2 < n < 3/4$. In this case the mechanism is exactly the same as the one above described for the strong-coupling limit of the KLM.[44] The mechanism that we describe below also operates in a mixed-valent situation ($|E_F - \epsilon_a| < |V|$) but for a different and more realistic region of parameters: $|V| \ll |t_b|$. Although both mechanisms could have common aspects, they also have important differences.

In Fig. 1, we illustrate the (one-dimensional) noninteracting bands for the case of interest: ϵ_a close to E_F and above the bottom of the b band. If $|V| \ll |t_b|$, we can identify two subspaces in each band where the states have either b (ψ subspace) or a (ϕ subspace) character. The size of the crossover region around the points where the original unhybridized b and a bands crossed is proportional to $|V/t_b|$; that is, it is very small. The creation operators for the Wannier orbitals $\psi_{\mathbf{r}\sigma}$ and $\phi_{\mathbf{r}\sigma}$ associated with each subspace are

$$\psi^\dagger_{\mathbf{r}\sigma} = \frac{1}{\sqrt{N}}\left[\sum_{\mathbf{k}\in\mathbf{K}^>} e^{i\mathbf{k}\cdot\mathbf{r}}\beta^\dagger_{\mathbf{k}\sigma} + \sum_{\mathbf{k}\in\mathbf{K}^<} e^{i\mathbf{k}\cdot\mathbf{r}}\alpha^\dagger_{\mathbf{k}\sigma}\right],$$

$$\phi^\dagger_{\mathbf{r}\sigma} = \frac{1}{\sqrt{N}}\left[\sum_{\mathbf{k}\in\mathbf{K}^>} e^{i\mathbf{k}\cdot\mathbf{r}}\alpha^\dagger_{\mathbf{k}\sigma} + \sum_{\mathbf{k}\in\mathbf{K}^<} e^{i\mathbf{k}\cdot\mathbf{r}}\beta^\dagger_{\mathbf{k}\sigma}\right], \tag{8}$$

where N is the number of sites. The subsets $\mathbf{K}^>$ and $\mathbf{K}^<$ are defined by $\mathbf{K}^> = \{\mathbf{k}: |u_{\mathbf{k}}| \geqslant |v_{\mathbf{k}}|\}$ and $\mathbf{K}^< = \{\mathbf{k}: |v_{\mathbf{k}}| > |u_{\mathbf{k}}\}$. Since the ψ and the ϕ subspaces are generated by eigenstates of H_0, it is clear that both subspaces can only be mixed by the interacting term H_U. Therefore in the new basis we have

$$H_0 = H_0^\phi + H_0^\psi = \sum_{\mathbf{r},\mathbf{r}',\sigma} \tau^\phi_{\mathbf{r}-\mathbf{r}'}\phi^\dagger_{\mathbf{r}\sigma}\phi_{\mathbf{r}'\sigma} + \sum_{\mathbf{r},\mathbf{r}',\sigma} \tau^\psi_{\mathbf{r}-\mathbf{r}'}\psi^\dagger_{\mathbf{r}\sigma}\psi_{\mathbf{r}'\sigma},$$

with the hoppings $\tau^\phi_{\mathbf{r}}$ and $\tau^\psi_{\mathbf{r}}$ given by the following expressions:

$$\tau^\phi_{\mathbf{r}} = \frac{1}{N}\left[\sum_{\mathbf{k}\in\mathbf{K}^>} e^{i\mathbf{k}\cdot\mathbf{r}}E^-_{\mathbf{k}} + \sum_{\mathbf{k}\in\mathbf{K}^<} e^{i\mathbf{k}\cdot\mathbf{r}}E^+_{\mathbf{k}}\right], \tag{9}$$

$$\tau^\psi_{\mathbf{r}} = \frac{1}{N}\left[\sum_{\mathbf{k}\in\mathbf{K}^>} e^{i\mathbf{k}\cdot\mathbf{r}}E^+_{\mathbf{k}} + \sum_{\mathbf{k}\in\mathbf{K}^<} e^{i\mathbf{k}\cdot\mathbf{r}}E^-_{\mathbf{k}}\right]. \tag{10}$$

The segmented structure of the ψ and the ϕ bands introduce oscillations in the hoppings $\tau^\psi_{\mathbf{r}}$ and $\tau^\phi_{\mathbf{r}}$ as a function of the distance $|\mathbf{r}|$.

Because the U term in H involves only the a orbitals, the matrix elements of H connecting the ϕ and ψ subspaces are small compared to the characteristic energy scales of the problem (the matrix elements of H within the subspaces). To see this we express $a^\dagger_{\mathbf{r}\sigma}$ as a function of $\phi^\dagger_{\mathbf{r}\sigma}$ and $\psi^\dagger_{\mathbf{r}\sigma}$ by first inverting Eqs. (6) and (8) to find

$$a^\dagger_{\mathbf{r}\sigma} = \sum_{\mathbf{r}'} W_{\mathbf{r}-\mathbf{r}'}\phi^\dagger_{\mathbf{r}'\sigma} + w_{\mathbf{r}-\mathbf{r}'}\psi^\dagger_{\mathbf{r}'\sigma}, \tag{11}$$

where the weights $W_{\mathbf{r}}$ and $w_{\mathbf{r}}$ are defined by

$$W_{\mathbf{r}} = \frac{1}{N}\left[\sum_{\mathbf{k}\in\mathbf{K}^>} e^{i\mathbf{k}\cdot\mathbf{r}}u_{\mathbf{k}} + \sum_{\mathbf{k}\in\mathbf{K}^<} e^{i\mathbf{k}\cdot\mathbf{r}}v_{\mathbf{k}}\right],$$

$$w_{\mathbf{r}} = \frac{1}{N}\left[\sum_{\mathbf{k}\in\mathbf{K}^>} e^{i\mathbf{k}\cdot\mathbf{r}}v_{\mathbf{k}} + \sum_{\mathbf{k}\in\mathbf{K}^<} e^{i\mathbf{k}\cdot\mathbf{r}}u_{\mathbf{k}}\right]. \tag{12}$$

The value of these weights as a function of the distance $|\mathbf{r}|$ is plotted in Fig. 2 (for $\epsilon_a = -1.5$, $V = 0.1t$, and $t_a = 0$). From Fig. 2 we can see that $W_{\mathbf{0}}$ is much larger than any other

weight. This is so because the ϕ orbitals have predominantly a character, while the ψ orbitals have mostly b character in the considered region of parameters. Therefore we can approximate the creation operator $a^{\dagger}_{\mathbf{r}\sigma}$ by

$$a^{\dagger}_{\mathbf{r}\sigma} \approx \sum_{\mathbf{r}'} W_{\mathbf{r}-\mathbf{r}'} \phi^{\dagger}_{\mathbf{r}\sigma}. \tag{13}$$

As a consequence of this approximation, the a subspace becomes invariant under the application of H. In addition, because $|W_{\mathbf{0}}| \gg |W_{\mathbf{r}\neq\mathbf{0}}|$ (see Fig. 2), we can establish a hierarchy of terms where the lowest order one corresponds to a simple on-site repulsion,

$$H^{U}_{eff} = \tilde{U} \sum_{\mathbf{r}} n^{\phi}_{\mathbf{r}\uparrow} n^{\phi}_{\mathbf{r}\downarrow}, \tag{14}$$

with $\tilde{U} = U|W_{\mathbf{0}}|^4$ and $n^{\phi}_{\mathbf{r}\sigma} = \phi^{\dagger}_{\mathbf{r},\sigma}\phi_{\mathbf{r},\sigma}$. The next order terms, containing three and two $W_{\mathbf{0}}$ factors, are much smaller and are essentially the same as the intersite interactions which in the past were added to the Hubbard model to enhance the ferromagnetism.[14]

Adding H^{U}_{eff} to H_0 we get the effective Hamiltonian

$$H_{eff} = \sum_{\mathbf{r},\mathbf{r}',\sigma} (\tau^{\psi}_{\mathbf{r}-\mathbf{r}'} \psi^{\dagger}_{\mathbf{r}\sigma}\psi_{\mathbf{r}'\sigma} + \tau^{\phi}_{\mathbf{r}-\mathbf{r}'} \phi^{\dagger}_{\mathbf{r}\sigma}\phi_{\mathbf{r}'\sigma}) + \tilde{U} \sum_{\mathbf{r}} n^{\phi}_{\mathbf{r}\uparrow} n^{\phi}_{\mathbf{r}\downarrow}. \tag{15}$$

The ψ and ϕ orbitals form uncorrelated and correlated nonhybridized bands: $H_{eff} = H^{\psi} + H^{\phi}$. For the ϕ orbitals we obtain an effective one band Hubbard model with the peculiar double-shell-like dispersion relation shown by the thick lines in Fig. 1.

Particularly for $t_a = 0$, H^{ϕ} has a very large density of states in the lower shell of the ϕ band[14] which is located near ϵ_a. From Fig. 1 it is also clear that the electrons first doubly occupy the uncorrelated ψ band states which are below ϵ_a. However, when the system becomes mixed valent because E_F gets close to ϵ_a, the electrons close to the Fermi level go into some of the correlated ϕ states. The interaction term H^{U}_{eff}, combined with the double shell band structure of H^{ϕ}_{0}, gives rise to a FM ground state (GS): The electrons close to E_F spread to higher unoccupied $\mathbf{k}$ states and polarize, which causes the spatial part of their wave function to become antisymmetric. This process eliminates double occupancy in real space and reduces the Coulomb repulsion to zero. The cost of polarizing is just an increase in the kinetic energy proportional to $\delta_a \sim \hbar v_F \delta_k$, where v_F is the Fermi velocity and δ_k is the interval in $\mathbf{k}$ space in which the electrons are polarized.

To determine the stability of this unsaturated FM state, we compare its energy with that of the PM state. If we were to build a nonmagnetic state with only the states of the lower ϕ shell, we would find a restricted delocalization for each electron because of the exclusion of the finite set of band states ($\mathbf{k}$ states) which belong to the upper shell. To avoid the Coulomb repulsion U for double occupying a given site, the electrons need to occupy all $\mathbf{k}$ states. This means they have to occupy the ϕ states in the upper and lower shells. This restricted delocalization is a direct consequence of Heisenberg's uncertainty principle, and the resulting localization length depends on the wave vectors where the original b and a bands crossed. These wave vectors define the size ($\Delta\mathbf{k}$) of each shell. The energy cost for occupying the ϕ states in the upper shell is proportional to the hybridization gap Δ, which for $|t_b| \ll |t_a|$ and $t_b > 0$ is given by

$$\Delta = D[\sqrt{(\epsilon_a/2 + Dt_a - Dt_b)^2 + V^2} - 2t_a + \sqrt{(\epsilon_a/2 + Dt_b - Dt_a)^2 + V^2} - 2t_b]. \tag{16}$$

Therefore if U is the dominant energy scale in the problem and $\Delta \gg \delta_a$, the FM state lies lower in energy than the nonmagnetic state. Under these conditions, the effective FM interaction is proportional to the hybridization gap Δ.

This mechanism for ferromagnetism on a lattice is analogous to the intra-atomic Hund's mechanism polarizing electrons in atoms. In atoms, we also have different degenerate (the equivalent of δ_a is zero) shells separated by an energy gap. If the valence shell is open, the electrons polarize to avoid the short-range part of the Coulomb repulsion (again reflecting the Pauli exclusion principle). The energy of an eventual nonmagnetic state is proportional either to the magnitude of the Coulomb repulsion or to the energy gap between different shells. The interplay between both energies sets the scale of Hund's intra-atomic exchange coupling.

IV. NUMERICAL METHOD

Our numerical method, the constrained-path Monte Carlo (CPMC) method, is extensively described and benchmarked elsewhere.[46,47] Here we only discuss its basic features, assumptions, and special details about our use of it.

In the CPMC method, the ground-state wave function $|\Psi_0\rangle$ is projected from a known initial wave function $|\Psi_T\rangle$ by a branching random walk in an overcomplete space of Slater determinants $|\phi\rangle$. In such a space, we can write $|\Psi_0\rangle = \Sigma_{\phi} c_{\phi} |\phi\rangle$, where $c_{\phi} > 0$. The random walk produces an ensemble of $|\phi\rangle$, called random walkers, which represent $|\Psi_0\rangle$ in the sense that their distribution is a Monte Carlo sampling of $c_{\phi}/\Sigma_{\phi} c_{\phi}$, that is, a sampling of the ground-state wave function.

To completely specify $|\Psi_0\rangle$, only determinants satisfying $\langle\Psi_0|\phi\rangle > 0$ are needed because $|\Psi_0\rangle$ resides in either of two degenerate halves of the Slater determinant space, separated by a nodal plane. In the CPMC method the fermion sign problem occurs because walkers can cross this plane as their orbitals evolve continuously in the random walk. Without *a priori* knowledge of this plane, we use a trial wave function $|\Psi_T\rangle$ and require $\langle\Psi_T|\phi\rangle > 0$. The random walk solves Schrödinger's equation in determinant space, but under an approximate boundary condition. This is what is called the constrained-path approximation.

The quality of the calculation depends on the quality of the trial wave function $|\Psi_T\rangle$. Fortunately, extensive testing has demonstrated a significant insensitivity of the results to reasonable choices: Since the constraint only involves the overall sign of its overlap with any determinant $|\phi\rangle$, some insensitivity of the results to $|\Psi_T\rangle$ is expected.[17,46–50]

Besides, as a starting point and as a condition constraining a random walker, we also use $|\Psi_T\rangle$ as an importance function. Specifically, we use $\langle\Psi_T|\phi\rangle$ to bias the random walk into those parts of Slater determinant space that have a large overlap with the trial state. For all three uses of $|\Psi_T\rangle$, it clearly is advantageous to have $|\Psi_T\rangle$ approximate $|\Psi_0\rangle$ as closely as possible. Only in the constraining of the path does $|\Psi_T\rangle \neq |\Psi_0\rangle$ in general generate an approximation.

We constructed $|\psi_T\rangle = \Pi_\sigma |\phi_T^\sigma\rangle$ from the eigenstates of the noninteracting problem. Because the total and z-component spin angular momentum, S and S_z, are good quantum numbers, we could choose unequal numbers of up and down electrons to produce trial states and hence ground states with $S = S_z = \frac{1}{2}(N_\uparrow - N_\downarrow)$. Whenever possible, we would simulate closed shells of up and down electrons, as such cases usually provided energy estimates with the least statistical error, but because we wanted to study the ground-state energy as a function of S, we frequently had to settle for just the up or down shell being closed. In some cases, the desired value of S could not be generated from either shell being closed. Also we would select the noninteracting states so $|\psi_T\rangle$ would be translationally invariant, even if these states used did not all come from the Fermi sea. The use of unrestricted Hartree-Fock eigenstates to generate $|\phi_T^\sigma\rangle$ instead of the noninteracting eigenstates generally produced no significant improvement in the results.

In particular, we represented the trial wave function as a single Slater determinant whose columns are the N_σ single-particle orbitals obtained from the exact solution of H_0. We chose the orbitals with lowest energies given by $E_{\mathbf{k}}^-$ and filled them up to a desired number of electrons N_e,

$$|\psi_T\rangle = \prod_{\mathbf{k},\sigma} \alpha_{\mathbf{k},\sigma}^\dagger |0\rangle, \tag{17}$$

where $|0\rangle$ represents a vacuum for electrons. Since our calculations were performed for a less than full lower band, only states from the lower band were used to construct the trial wave function.

In a typical run we set the average number of random walkers to 400. We performed 2000 Monte Carlo sweeps before we taking measurements, and we made the measurements in 40 blocks of 400 steps. By choosing $\Delta\tau = 0.05$, we reduced the systematic error associated with the Trotter approximation to be smaller than the statistical error. In measuring correlation functions, we performed between 20 and 40 back-propagation steps.

V. QUANTUM MONTE CARLO RESULTS

In Sec. III, we have described a mechanism for itinerant ferromagnetism which is present in the mixed-valence regime for $n > 1/4$. In addition, we mentioned that the system is also expected to be FM when the a magnetic moments are localized ($|V| \ll |E_F - \epsilon_a|$) because the effective Ruderman-Kitted-Kasuya-Yasida (RKKY) coupling is negative when the Fermi surface is small ($k_F \sim 0$). In this section we show that the itinerant and the localized ferromagnetic states are continuously connected in the phase diagram of the PAM. However, the energy scale of the first state is much larger than the RKKY interaction which characterizes the second one. The existence of a crossover region between both states could explain the fact that there are some f-electron compounds for which it is very difficult to determine whether they are itinerant or localized ferromagnets. Note that if ϵ_a is increased continuously from the localized limit ($\epsilon_a < -2D|t_b|$), the Fermi level practically does not change at the beginning. However, when ϵ_a reaches E_F, the Fermi level starts to follow ϵ_a until all the a electrons are completely transferred from the a to the b band. Concomitantly, the character of the conduction electrons changes continuously, first from b to a and later from a back to b. Most of the results that we include below correspond to this region of parameters.

In addition, we will see that the QMC results for H [Eq. (1)] are consistent with the simple picture derived from our effective model [Eq. (15)]. According to that picture, the ferromagnetic state in the mixed-valence regime should be similar to a partially polarized noninteracting solution where the polarized electrons are the ones occupying the a-character orbitals. It is only in the crossover region of size $V^2/|t_b|$ (see Fig. 1), where the orbitals have a mixed character, that the correlations introduce an appreciable effect. This effect is the well-known Kondo-like singlet correlation between the b and the a electrons. However, it is important to remark that these Kondo singlets only exist in an energy interval V^2/W (where W is the d bandwidth), and therefore the number of Kondo singlets N_{KS} is much smaller than the number of magnetic moments N_{MM}: $N_{KS}/N_{MM} \sim V^2/W^2$. This is a simple manifestation of the ''exhaustion'' phenomenon described by Nozierés.[51,52] Since most of the a magnetic moments are ferromagnetically polarized, the role of these few Kondo singlets is marginal in our FM solution. Therefore, for the mixed-valence regime with $n > 1/4$, the a magnetic moments which are not screened by b electrons develop an effective magnetic interaction as a consequence of the interplay between the local Coulomb interaction and the particular band structure. In other words, the ''collective Kondo state'' which was proposed in the past[51,52] is replaced by band ferromagnetism.[53]

In fact, the nature of local moment compensation in the PAM differs qualitatively from that in the single impurity Anderson model.[17] In the PAM, if the ground state is a singlet, then

$$\langle S_a^z(j)^2\rangle = -\sum_i \langle S_b^z(i) S_a^z(j)\rangle - \sum_i \langle S_a^z(i) S_a^z(j)\rangle. \tag{18}$$

In the impurity model, the last term is absent, and the resulting expression is the analytic statement of the well-known Clogston-Anderson compensation theorem that express the compensation of the a moment by the conduction electrons. In the PAM, on the other hand, the last term dominates the first so the a moment is compensated largely by correlations induced among themselves.

To understand the nature of the FM solution, we plotted the mean occupation number of the quasiparticle operators which diagonalize the noninteracting problem [see Eq. (5)].

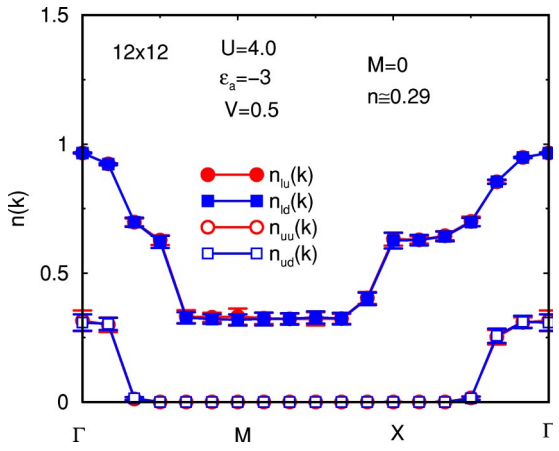

FIG. 3. Mean values of the quasiparticle occupation numbers for the noninteracting band states for the paramagnetic $S=0$ solution of the PAM in a two-dimensional lattice. Legends: $n_{lu}(\mathbf{k})$ represents lower-band occupation number of up spins, $n_{ud}(\mathbf{k})$ represents upper-band occupation number of down spins, etc.

This is shown in Fig. 3 for the lowest energy PM ($S=0$) state in a two-dimensional cluster of 12×12 unit cells. We can see that the *b*-character states of the lower band are close to being doubly occupied. In contrast, the *a*-character region has a smaller occupation number (~0.7). It is remarkable that the populations of the *a*-character states in the lower and the upper bands are very similar. This delocalization in the momentum space is a direct consequence of the tendency to avoid double occupancy in the real space. This indicates that the energy increase of the PM state due to the inclusion of U is proportional to the hybridization gap Δ.

Figure 4 shows the quasiparticle occupation numbers for the partially saturated FM ground state. While the *b*-character states of the lower band are still close to being doubly occupied, the *a*-character ones are polarized and the occupation number is 1 for any of them. The occupation number for the *a*-character states in the upper band is much smaller than the corresponding one for the PM solution (see

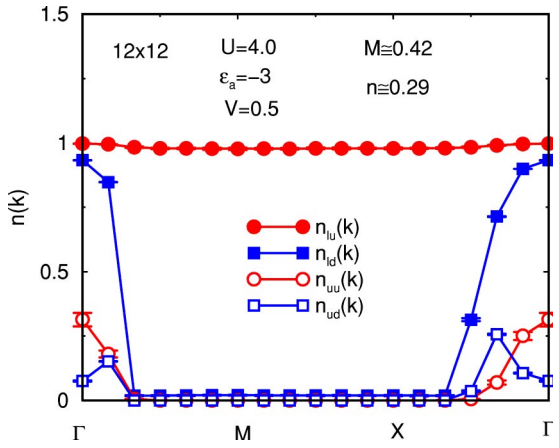

FIG. 4. Mean values of the quasiparticle occupation numbers for the noninteracting band states for the ground state (partially saturated ferromagnet with $M=S/N=0.43$) of the PAM in a two-dimensional lattice.

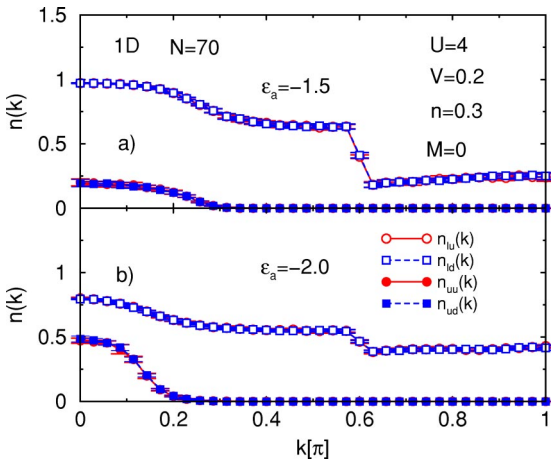

FIG. 5. Mean values of the quasiparticle occupation numbers for the noninteracting band states for the paramagnetic $S=0$ solution of the PAM in a chain.

Fig. 3). This difference can be understood in the following way: the polarized *a* electrons can localize in momentum space because the Pauli exclusion principle prevents double occupancy in real space (the spatial wave function is completely antisymmetric). Therefore the *a* electrons do not need to occupy the upper band states and the energy increase due to the repulsive U term is proportional to $\hbar v_F \delta_k$. The nonzero amount of electrons occupying the center of the upper band (see Fig. 4) comes from the crossover regions for which the *a* and the *b* character of the states are comparable. Since the electrons occupying these states are not polarized, the effect of the Coulomb repulsion U is the transfer of spectral weight from the lower to the upper band to avoid double occupancy in real space.

We can see from Figs. 5 and 6 that a similar behavior is obtained for one-dimensional systems. As it follows from Sec. III, the mechanism for this ferromagnetism works in any finite dimension. Notice in Fig. 5 that there is a jump in the occupation number of the lower band as a function of **k**. The inverse of this jump is proportional to effective mass of the

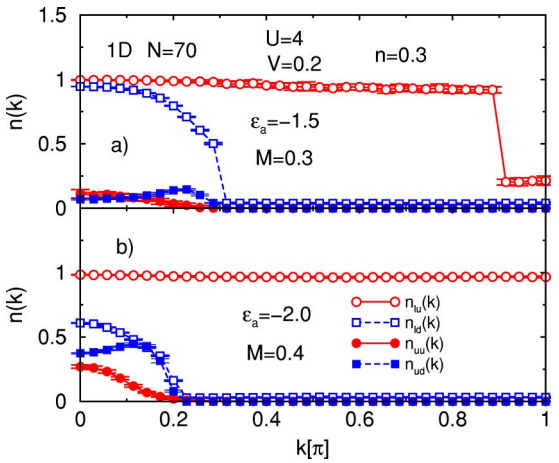

FIG. 6. Mean values of the quasiparticle occupation numbers for the noninteracting band states for the ground state (partially saturated ferromagnet with $M=S/N=0.3$) of the PAM in a chain.

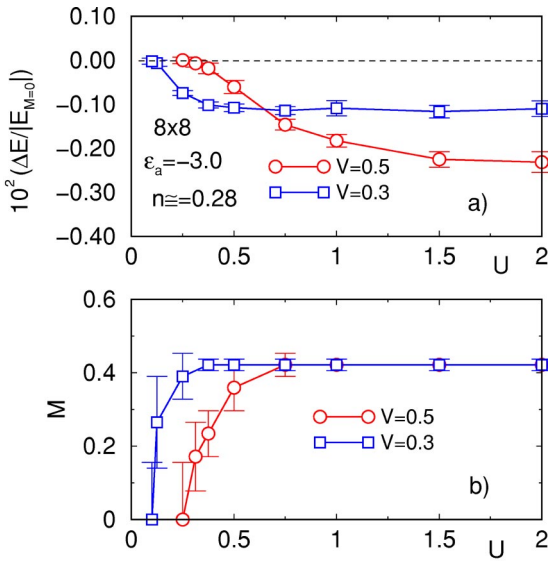

FIG. 7. (a) Energy difference between partially polarized FM ground state and the lowest energy paramagnetic state as a function of U. (b) Magnetization as a function of U.

quasiparticles of the paramagnetic solution. When ϵ_a decreases, the system evolves into a state where the a electrons are localized. This evolution is reflected in the decrease of the jump and the consequent increase of the effective mass.

For $U=0$ the system is a PM metal. We then expect a critical value of the on-site repulsion U_c separating the PM from the FM region. From Fig. 7, the value obtained for U_c is $U_c \sim 0.25 \sim \Delta = 0.242$ for $V=0.5$ and $U_c \sim 0.11 \sim \Delta = 0.0981$ for $V=0.31$ ($\epsilon_a = -3$). This is also in agreement with the mechanism described in Sec. III. If $\Delta \gg \delta_a$ and U becomes larger than the hybridization gap Δ, the system evolves into a FM state to avoid the double occupancy without an increase in the kinetic energy proportional to the hybridization gap.

According to Figs. 7(b) and 8 the magnetization seems to increase gradually when U is increased beyond its critical value. This behavior suggests that the FM transition as function of U is of second order. If this is so, the properties of the PM Fermi liquid which is obtained for $U<U_c$ should be strongly affected by the FM fluctuations when U approaches U_c. It is known that the effective mass of the quasiparticles

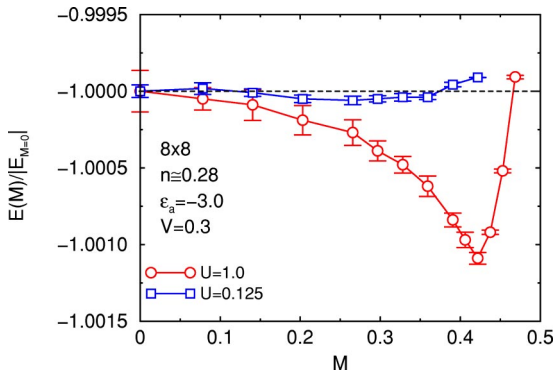

FIG. 8. Minimum energy as a function of the magnetization.

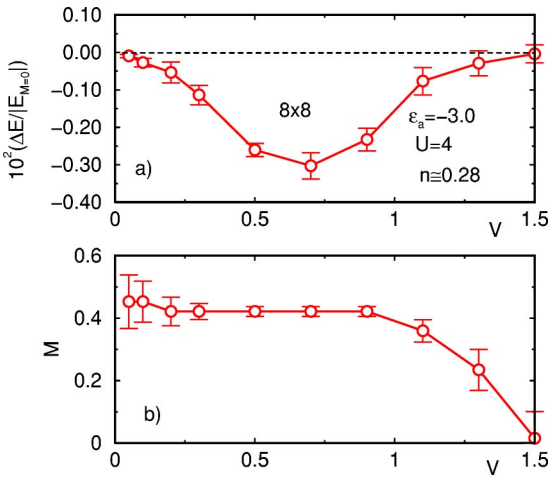

FIG. 9. (a) Energy difference between the FM ground state and the lowest energy paramagnetic state as a function of V. (b) Magnetization as a function of V.

diverges in the approach to a zero-temperature ferromagnetic instability.[54–57] In other words, the behavior of the PM Fermi liquid cannot be understood by analogy with the one impurity problem. The Kondo temperature, which is the characteristic energy scale of the one impurity problem, is replaced by a new Fermi temperature which is dominated by the ferromagnetic fluctuations and goes to zero when U approaches to U_c from below.

Another relevant parameter for the FM solution is the hybridization V. For $V=0$ and $\epsilon_a = E_F$ there is a complete spin degeneracy for the electrons occupying the localized a orbitals. By increasing V, we are simultaneously changing the Fermi velocity v_F and the hybridization gap Δ. For small values of V, Δ is much larger than $\delta_a = \hbar v_F \delta_k$ in the region under consideration. For this reason, a nonzero value of V removes the original spin degeneracy stabilizing the partially polarized FM solution (see Fig. 9). When V is larger than t, the two relevant energy scales Δ and δ_a become of the same order and the partially polarized FM is replaced by a PM phase. In the unrealistic large V limit ($|V| \gg |t_b|, U, |\epsilon_a|$), the ground state consists of local Kondo singlets moving in a background of localized spins.

Finally, the most sensitive parameter for the stabilization of the FM state is the difference $|\epsilon_a - E_F|$. In Fig. 10, we show the energy difference ΔE between the FM ground state and the lowest energy PM ($S=0$) state as a function of ϵ_a. When ϵ_a is considerably smaller than E_F, the a electrons are localized and the magnetism is dominated by the RKKY interaction. The order of this interaction is V^4. This gives the small value of $|\Delta E|$ when the a levels are below the bottom of the conduction band: $\epsilon_a < -2D|t_b|$. The most stable region for the FM state (maximum value of $|\Delta E|$) starts when ϵ_a reaches the Fermi level. For the case of Fig. 10, this occurs at $\epsilon_a \sim -1.9$. Again this result is in agreement with the mechanism described in Sec. III. If we continue increasing the value of ϵ_a, the number of a electrons decreases and the magnetization is consequently reduced [see Fig. 10(b)]. Note that when ϵ_a reaches the Fermi level, it remains practically equal to E_F until all the a electrons are transferred to

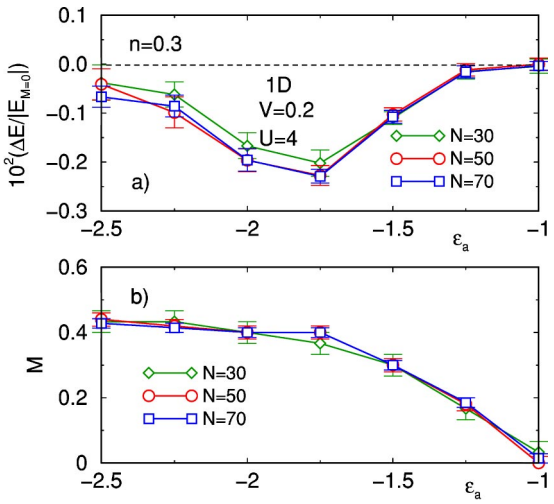

FIG. 10. (a) Energy difference between FM ground state and the lowest energy paramagnetic state as a function of ϵ_a for a one-dimensional system. (b) Magnetization as a function of ϵ_a.

the b band. Finally, when ϵ_a becomes larger than E_F, the magnetization goes to zero in a smooth way indicating that the associated quantum phase transition is of second order.

Figure 11 shows the ϵ_a dependence of ΔE for two- and three-dimensional clusters. As in the one-dimensional case, the stability of the FM phase increases when the system approaches the mixed-valence regime. The qualitative behavior of $|\Delta E|$ and M does not depend on the dimensionality of the system for $D \leqslant 3$. It is remarkable that in the mixed-valence regime, the stabilization energy $|\Delta E|$ is one order of magnitude larger than the corresponding value in the localized regime.

To validate our results in the thermodynamic limit it is necessary to do finite-size scaling. Because there are very few (nontilted) square super cells where identical dopings away from half filling are realized as the cell size is varied, we usually used tilted cells. (Nontilted cell of size $N=m^2$ have m lattices points on the cell edges.) The necessary condition for the existence of a tilted square super cell with N sites that tiles space is: $N=l^2+m^2$, where l and m are

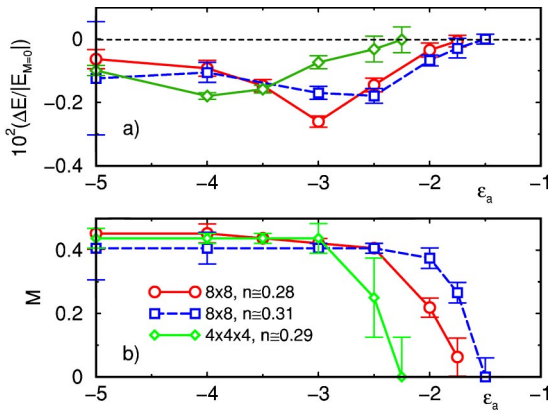

FIG. 11. (a) Energy difference between FM ground state and the lowest energy paramagnetic state as a function of ϵ_a for two- and three-dimensional systems. (b) Magnetization as a function of ϵ_a.

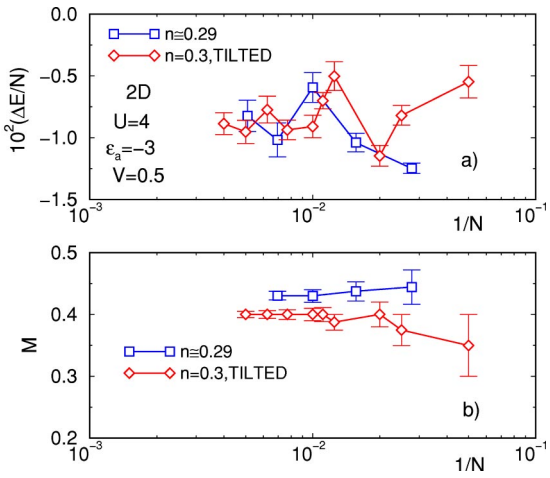

FIG. 12. (a) Scaling of the energy difference between the FM ground state and the lowest energy paramagnetic state for two-dimensional systems. (b) Scaling of the magnetization per site.

integers.[58] For the doping of $n=0.3$, we used tilted cells for $N=20$, 40, 50, 80, 90, 100, 130, 160, 200, and 250. For $N=100$ a tilted and nontilted cell exists. In Fig. 12, we show the scaling of ΔE and the magnetization per site for a two-dimensional system. The finite-size effects are stronger in two-dimensional systems. (For one-dimensional scaling results, see Fig. 2 in Ref. 1.)

We show two different cases: the circles correspond to a sequence of tilted square clusters which allows us to fix the concentration in $n=0.3$; the squares correspond to a sequence of untilted square clusters for which the value of the concentration is the closest to $n=0.29$. Despite the considerable size effects, these results indicate that the FM state is stable in the thermodynamic limit. In this case, the extrapolated magnetization is close to 0.4.

Meyer and Nolting[30] have also found a FM solution for the PAM in a similar region of parameters using DMFT. However, it is important to remark that the mechanism for ferromagnetism described in Sec. III works only in finite dimension. In any dimension, the fundamental problem is correctly estimating the energy of the paramagnetic state relative to the ferromagnetic state. For two parallel spins, the Pauli exclusion principle is a natural mechanism for preventing the electrons from incurring a high Coulomb energy cost by occupying the same site. On the other hand, two antiparallel spins have to develop spatial correlations to prevent this. Properly computing these correlations is one essential requirement for a predictive theory and the most difficult part of the problem. Typically, mean-field theory in any finite dimension is unable to capture these correlations adequately enough. To have a ferromagnetic state, a second requirement is the development of an energy scale to prevent the paramagnetic state with adequate spatial correlations from having a lower energy than the ferromagnetic state. In the mechanism for ferromagnetism just presented, the quantum Monte Carlo method allowed the proper computation of the spatial correlations to permit the accurate determination of the energies of both the paramagnetic and ferromagnetic states. What is interesting about the mechanism is the observation

that band structure of the noninteracting problem sets an energy scale Δ that for a range of electron densities makes the formation of the paramagnetic state more costly than the ferromagnetic state even when the spatial correlations are developed in the former one.

In infinite dimension, a number of things are different. For one thing, the physics becomes local as the self-energy is independent of wave number. As a consequence, spatial correlations cannot develop. The absence of spatial correlation avoiding double occupancy of sites leads to the paramagnetic state naturally tending to have a higher energy than the ferromagnetic state, and the absence of the energy scale associated with band features leaves the appearance of the ferromagnetic state being principally a consequence of a very high density of state near the Fermi energy. When the infinite dimensional physics is used to approximate the physics of finite dimensions by what is called DMFT, a high density of states near the Fermi energy, as is the case in the mixed-valence regime, promotes the ferromagnetic state. This is also reflected by the fact that the energy scale (T_C) of the FM solution found with DMFT for the localized regime is larger than the one for the mixed-valence regime (region IV of Ref. 28). This behavior is opposite to our result (see Fig. 10).

VI. EXPERIMENTAL CONSEQUENCES

A. Cerium compounds

During the last few years experimental results have confirmed that there are Ce based compounds which cannot be treated as typical Kondo systems. For instance, $CeRh_3B_2$ has a very high FM ordering temperature ($T_C = 115$ K) which sticks out from a localized $4f$-electron description.[59] In addition the alloy series $Ce(Rh_{1-x}Ru_x)_3B_2$ (Ref. 59) and $La_xCe_{1-x}Rh_3B_2$ (Ref. 60) exhibit many unusual characteristics which require a new macroscopic description with respect to the competition among classical Kondo versus RKKY interactions.[38]

Absorption edge spectroscopy measurements of $Ce(Rh_{1-x}Ru_x)_3B_2$ for different values of x indicate that the stoichiometric compound $CeRh_3B_2$ is in the mixed-valence regime (fluctuating between the $4f^1$ and the $4f^0$ configurations).[59] After doping with Ru, there is a strong transfer of weight from the $4f^1$ line to the $4f^0$ structure. This change can be understood in the context of the PAM if we take into account that the volume of the system decreases when Rh is replaced by Ru.[60] In this situation the width of the conduction band increases and some f (a) electrons are transferred to d (b) character orbitals (see Fig. 1). According to our results this change must decrease the value of the zero-temperature magnetization and the Curie temperature T_C. By increasing the doping level we can reach a situation where most of the f electrons that were polarized in the stoichiometric compound are transferred to the d character orbitals and the zero-temperature magnetization is very small. In this limit the system should be a weak ferromagnet because there are very few f (a) electrons close to the Fermi level (see Fig. 1). When the energy difference between the Fermi level and the f level (ϵ_a) becomes smaller than T_C, the magnetization can increase with temperature because the number of f (a) electrons increases. The electrons which are occupying the PM d (b) states near the Fermi level are thermally promoted to the f character states which are just above the Fermi level. In this process, the electrons are polarized because of the mechanism discussed above. This explains the finite temperature peak in the magnetization of $Ce(Rh_{1-x}Ru_x)_3B_2$ (for x between 0.06 and 0.125) (Refs. 59 and 61) that suggests an ordered state with high entropy. The source of the large entropy is thus associated with charge and not with spin degrees of freedom which is why a state with larger M has a higher entropy. From this analysis we predict that the integral of the entropy below T_C, which can be extracted from the specific-heat measurements, contains a considerable contribution from the *charge* degrees of freedom.

When Ce is replaced by La, the volume of the system increases[60] and the magnetic moments become more localized. In this case, the weight in the absorption edge spectroscopy is transferred from the $4f^0$ structure to the $4f^1$ line. Again this can be understood if we take into account that the width of the conduction band decreases in this case and the electrons are transferred from the d to the f character orbitals (see Fig. 1). In this way the system evolves from the itinerant to the localized situation ($\epsilon_f = \epsilon_a < E_F$). According to our results (see Fig. 10), this change should increase the value of the zero-temperature magnetization and simultaneously decrease the Curie temperature T_C [$|\Delta E|$ is strongly reduced because the effective magnetic interaction in the localized limit, J_{RKKY}, is order V^4 (Ref. 1)]. This anomalous behavior has been experimentally observed by Shaheen *et al.*[60] in $La_xCe_{1-x}Rh_3B_2$.

We can also connect our mechanism with the hydrostatic pressure dependence of T_C. To do this we calculated $|\Delta E|/N$ by the QMC method as function of increasing t_b. Here we are assuming that the main effect of the hydrostatic pressure is to increase t_b and to leave the other parameters unchanged. The order of magnitude of $|\Delta E|/N$, which should be proportional to T_C, and its qualitative behavior are in good agreement with the experimental results for $CeRh_3B_2$.[10] We can see from Fig. 3(a) in Ref. 1 that for the itinerant FM case, $|\Delta E|/N$ is of the order of 100 K. This scale is much larger than the magnitude of the RKKY interaction[62] (~ 1 K) which is commonly used to explain the origin of the magnetic phase when the a electrons are localized.

B. Uranium compounds

The FM uranium monochalcogenides US, USe, and UTe are semimetals with large Curie temperatures of $T_C = 180$, 160, and 108 K and ordered moments of 1.5, 2.0, and $2.2\mu_B$, respectively.[63] Most of the magnetic properties of these systems are still unexplained. The purpose of this subsection is to argue that the mechanism for ferromagnetism introduced above is a good candidate to explain some of the mysteries related to these compounds.

Erdös and Robinson[64] suggested that the uranium monochalcogenides are mixed-valence systems. This sugges-

tion was reinforced by measuring the Poisson ratio as a function of the chalcogen mass with low-temperature ultrasonic studies on USe and UTe.[65] The coexistence of an intermediate-valence regime and ferromagnetism is one of the unexplained properties of these compounds as it is recognized in Ref. 63. According to the traditional picture,[38] the system should behave as a nonmagnetic collective Kondo state in the intermediate-valence regime. In contrast to this picture, our results show that a partially saturated ferromagnetic state is stabilized in the mixed-valence regime. This can explain the first striking property of the uranium monochalcogenides.

The other unusual property of these compounds is the shape of the magnetization curve versus temperature which has a maximum below T_C.[64] Again this is a property which can be easily explained (see the subsection about the Ce compounds) within the context of the PAM. In addition, the order of magnitude of the Curie temperature of these compounds coincides with the energy scale obtained from the PAM for the intermediate-valence regime.

The uranium monochalcogenides, like the Ce based compounds above described, exhibit a nonmonotonic behavior for the T_C as a function of pressure.[10] Figure 3(b) in Ref. 1 shows that this behavior can also be explained with the PAM. Notice, however, that the nonmonotonic behavior shown in this figure has nothing to do with a competition between the Kondo and RKKY energy scales.

Finally, the spin-wave dispersions of these compounds also present some anomalies. For instance, neutron-scattering experiments on a single-domain UTe crystal[66,67] show that for wave vectors q perpendicular to the ordered moment the excitations become more damped with increasing q. In US only a broad continuum of magnetic response is observed.[68] Damped and unpolarized spin waves are observed in USe.[69–71] These properties indicate that the itinerant character of the f electrons is essential to have a good description of the magnetic excitations.

C. Transition metals

Even though the transition metals are the most well studied itinerant ferromagnets, the ultimate reason for the stabilization of the FM phase is still unknown. Since the minimal correlated model (Hubbard Hamiltonian) proposed to describe these systems does not seem to have a FM solution, it is reasonable to ask whether an extension of this minimal model, including more than one band, is necessary and sufficient to stabilize the FM solution. The correlated $3d$ band of the transition metals is hybridized with weakly correlated and dispersive s and p bands. This situation is similar to the case already described for the f electron compounds. Therefore it is natural to ask if there is a connection between the itinerant ferromagnetism of the f and the d electron compounds. Notice that the order of magnitude of the T_C is the same. Following the same motivation and using DMFT, Schwieger and Nolting[35] concluded that the d-band ferromagnetism can be stabilized when the hybridization between both bands is small. However, these authors also find a FM solution for the one band problem.

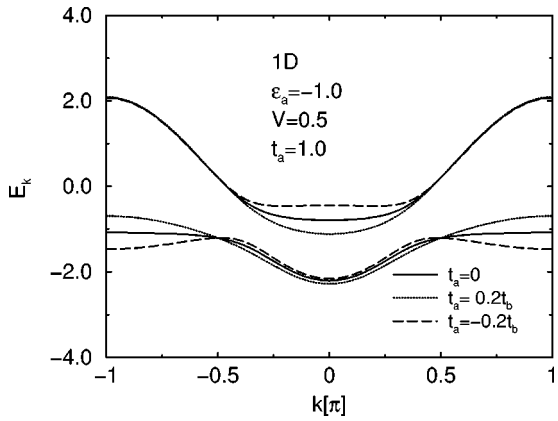

FIG. 13. One-dimensional band structure for different values of t_a.

In the case of the transition metals, the dispersion of the narrower band $(3d)$ cannot be neglected. For this reason, we studied the stability of the FM solution as a function of t_a. We can see from Fig. 3(b) of Ref. 1 that the FM phase is even more stable for $t_a \sim -0.1$ than for $t_a = 0$ and becomes unstable for $t_a \sim 0.05$. The reason for this asymmetric behavior is easy to understand in terms of the variation of δ_a: If t_a is negative, then the effect of t_a on the dispersion of the ϕ band is opposite to that of the hybridization V (see Fig. 13). When $t_a \sim -0.1$, we get, for the given ϵ_a and V, the minimum value for δ_a/Δ and therefore the most stable FM case. When we depart from this value of t_a, δ_a/Δ increases, $|\Delta E|$ decreases, and the FM state becomes less stable.

This result indicates that the hybridization between bands can play a crucial role for the ferromagnetism of the iron group. In other words, the ferromagnetism of the transition metals can originate, at least in part, in the interplay between the correlations and the particular band structure and not solely in the intra-atomic Hund's exchange.[5]

VII. CONCLUSIONS

We introduced a different mechanism for itinerant ferromagnetism which is present in a simple two band model consisting of a narrow correlated band hybridized with a dispersive and uncorrelated one. The picture just presented, combined with our previous results,[1] allows a reconciliation of the localized and delocalized ferromagnetism pictures painted by Heisenberg[72] and Bloch.[73] The hybridization between bands and the particular band structure play a crucial role in this mechanism because they generate a multishell structure for the correlated orbitals. This structure, when combined with a local Coulomb repulsion, favors a ferromagnetic state. The mechanism is analogous to the one which generates the atomic Hund interaction. In this sense, this is a generalization to the solid of the atomic Hund's rule. The mechanism works in any finite dimension.

The determination of a minimal model to explain the metallic ferromagnetism of highly correlated systems has been the object of intense effort during the last 40 years. The results presented in this paper suggest that the PAM is a minimal Hamiltonian which can explain the itinerant ferro-

magnetism without including any explicit FM interaction.

Another important aspect of this ferromagnetic solution is its mixed-valence character. According to the traditional picture,[38] the mixed-valence regime should be a PM Kondo state. The appearance of a ferromagnetic instability in this region of doping rises some questions about the entire validity of a Kondo-like description inspired by the one impurity problem. Even the PM phase obtained for $U<U_c$ is strongly influenced by the proximity to a FM instability.[54–57]

We have discussed the relevance of these results for some *f*-electron compounds which are itinerant ferromagnets with high Curie temperatures ($\sim$100 K). In particular, there are several unusual characteristics of the Ce based compounds $Ce(Rh_{1-x}Ru_x)_3B_2$ and $La_xCe_{1-x}Rh_3B_2$, and the uranium monochalcogenides US, USe, and UTe, which can be explained, at least at a qualitative level, with the present mechanism.

We have also considered the case relevant for the iron group where the dispersion of the lower band is not negligible. The fact that the ferromagnetism is even more stable for finite values of t_a when the hoppings of both bands have opposite signs indicates that our mechanism is relevant to explain the ferromagnetism of the transition metals, like Ni, where a correlated and narrow $3d$ band is hybridized with the $4s$ band. It suggests that the ferromagnetism in the transition metals can originate, at least in part, in the interplay between the correlations and the particular band structure, and not solely in the intra-atomic Hund's exchange.[5]

ACKNOWLEDGMENTS

This work was sponsored by the US DOE. We acknowledge useful discussions with A. J. Arko, B. H. Brandow, J. J. Joyce, G. Lander, J. M. Lawrence, S. Trugman, G. Ortiz, and J. L. Smith. We thank J. M. Lawrence for pointing out the experimental work on the Ce compounds. J.B. acknowledges the support of Slovene Ministry of Education, Science and Sports and FERLIN.

[1] C.D. Batista, J. Bonča, and J.E. Gubernatis, Phys. Rev. Lett. **88**, 187203 (2002).
[2] J.C. Slater, Phys. Rev. **49**, 537 (1936); **49**, 931 (1936).
[3] E.C. Stoner, Proc. R. Soc. London, Ser. A **165**, 372 (1938); **169**, 339 (1939).
[4] E.P. Wohlfarth, Rev. Mod. Phys. **25**, 211 (1953).
[5] J.H. van Vleck, Rev. Mod. Phys. **25**, 220 (1953).
[6] J.C. Slater, Phys. Rev. **49**, 537 (1936).
[7] M.C. Gutzwiler, Phys. Rev. Lett. **10**, 59 (1963).
[8] J. Hubbard, Proc. R. Soc. London, Ser. A **266**, 238 (1963).
[9] J. Kanamori, Prog. Theor. Phys. **30**, 275 (1963).
[10] A.L. Cornelius and J.S. Schilling, Phys. Rev. B **49**, 3955 (1994).
[11] Y. Nagaoka, Phys. Rev. **147**, 392 (1966).
[12] E.H. Lieb, Phys. Rev. Lett. **62**, 1201 (1988).
[13] E.H. Lieb and D.C. Mattis, Phys. Rev. **125**, 164 (1962).
[14] D. Vollhardt, N. Blumer, K. Held, M. Kollar, J. Schlipf, and M. Ulmke, Z. Phys. B: Condens. Matter **103**, 283 (1997); J. Wahle, N. Blumer, J. Schlipf, K. Held, and D. Vollhardt, Phys. Rev. B **58**, 12 749 (1998).
[15] F. Becca and S. Sorella, Phys. Rev. Lett. **86**, 3396 (2001).
[16] R. Hlubina, S. Sorella, and F. Guinea, Phys. Rev. Lett. **78**, 1343 (1997).
[17] J. Bonča and J.E. Gubernatis, Phys. Rev. B **58**, 6992 (1998).
[18] C.D. Batista, J. Bonča, and J.E. Gubernatis, Phys. Rev. B **63**, 184428 (2001).
[19] M. Guerrero and R.M. Noack, Phys. Rev. B **53**, 3707 (1996).
[20] M. Guerrero and R.M. Noack, Phys. Rev. B **63**, 144423 (2001).
[21] B. Möller and P. Wölfe, Phys. Rev. B **48**, 10 320 (1993).
[22] Roman Doradziński and Jozef Spalek, Phys. Rev. B **56**, 14 239 (1997).
[23] Roman Doradziński and Jozef Spalek, Phys. Rev. B **58**, 3293 (1998).
[24] M. Jarrell, Phys. Rev. B **51**, 7429 (1995).
[25] A.N. Tahvildar-Zadeh, M. Jarrell, and J.K. Freericks, Phys. Rev. B **55**, R3332 (1997).
[26] A.N. Tahvildar-Zadeh, M. Jarrell, and J.K. Freericks, Phys. Rev. Lett. **80**, 5168 (1998).
[27] N.S. Vidhyahiraja, A.N. Tahvildar-Zadeh, M. Jarrell, and H.R. Krishnamurthy, Europhys. Lett. **49**, 459 (2000).
[28] D. Meyer, W. Nolting, G.G. Reddy, and A. Ramakanth, Phys. Status Solidi B **208**, 473 (1998).
[29] D. Meyer and W. Nolting, Phys. Rev. B **61**, 13 465 (2000).
[30] D. Meyer and W. Nolting, Phys. Rev. B **62**, 5657 (2000).
[31] D. Vollhardt, *The Mott Metal-Insulator Transition*, Springer-Verlag Tracts in Modern Physics Vol. 137 (Springer-Verlag, Berlin, 1997).
[32] T. Pruschke, M. Jarrell, and J.K. Freericks, Adv. Phys. **44**, 187 (1995).
[33] A. Georges, G. Kotliar, W. Krauth, and M. Rozenberg, Rev. Mod. Phys. **68**, 13 (1996).
[34] J.W. Rasul, Phys. Rev. B **61**, 15 246 (2000).
[35] S. Schwieger and W. Nolting, Phys. Rev. B **64**, 144415 (2001).
[36] P. Fulde, J. Keller, and G. Zwicknagl, *Solid State Physics*, edited by H. Ehrenreich and D. Turnbull (Academic, New York, 1990), Vol. 41, p. 1; H. R. Ott, in *Progress in Low Temperature Physics*, edited by D. F. Brewer (North-Holland, Amsterdam, 1987), Vol. XI, p. 215.
[37] J.R. Schrieffer and P.A. Wolff, Phys. Rev. **149**, 4910 (1966).
[38] S. Doniach, Physica B **91**, 231 (1977).
[39] R. Jullien, P. Pfeuty, A.K. Bhattacharjee, and B. Coqblin, J. Appl. Phys. **50**, 7555 (1979).
[40] P. Santini and J. Sólyom, Phys. Rev. B **46**, 7422 (1996).
[41] P. Fazekas and E. Müller-Hartmann, Z. Phys. B: Condens. Matter **85**, 285 (1991).
[42] H. Tsunetsugu, M. Sigrist, and K. Ueda, Rev. Mod. Phys. **69**, 809 (1997).
[43] C. Lacroix, Solid State Commun. **54**, 991 (1985).
[44] M. Sigrist, H. Tsunetsugu, K. Ueda, and T.M. Rice, Phys. Rev. B **46**, 13 838 (1992).
[45] C. D. Batista, J. Bonča, and J. E. Gubernatis, Phys. Rev. B **68**, 064403 (2003).

[46] S. Zhang, J. Carlson, and J.E. Gubernatis, Phys. Rev. Lett. **74**, 3652 (1995).
[47] S. Zhang, J. Carlson, and J.E. Gubernatis, Phys. Rev. Lett. **74**, 3652 (1995); Phys. Rev. B **55**, 7464 (1997); J. Carlson, J.E. Gubernatis, G. Ortiz, and Shiwei Zhang, *ibid.* **59**, 12 788 (1999).
[48] M. Guerrero, J.E. Gubernatis, and S. Zhang, Phys. Rev. B **57**, 11 980 (1998).
[49] M. Guerrero, G. Ortiz, and J.E. Gubernatis, Phys. Rev. B **59**, 1706 (1999).
[50] M. Guerrero, G. Ortiz, and J.E. Gubernatis, Phys. Rev. B **62**, 600 (2000).
[51] P. Noziéres, Ann. Phys. (Paris) **10**, 19 (1985).
[52] P. Noziéres, Eur. Phys. J. B **6**, 447 (1998).
[53] P. Fazekas, Philos. Mag. B **76**, 797 (1997).
[54] W.F. Brinkman and T.M. Rice, Phys. Rev. B **2**, 4302 (1970).
[55] D. Vollhardt, Rev. Mod. Phys. **56**, 99 (1984).
[56] M.T. Bal-Monod, Physica B & C **109 & 110B**, 1837 (1982).
[57] T. Moriya and J. Kawabata, J. Phys. Soc. Jpn. **34**, 639 (1973); **35**, 669 (1973).
[58] See, for example, J. Jaklic and P. Prelovsek, Adv. Phys. **49**, 1 (2000).
[59] S. Berger, A. Galatanu, G. Hilscher, H. Michor, Ch. Paul, E. Bauer, P. Rogl, M. Gómez-Berisso, P. Pedrazzini, J.G. Sereni, J.P. Kappler, A. Rogalev, S. Matar, F. Weill, B. Chevalier, and J. Etourneau, Phys. Rev. B **64**, 134404 (2001).
[60] S.A. Shaheen, J.S. Schilling, and R.N. Shelton, Phys. Rev. B **31**, 656 (1985).
[61] S.K. Malik, A.M. Umarji, G.K. Shenoy, P.A. Montano, and M.E. Reeves, Phys. Rev. B **31**, 4728 (1985).
[62] P.-G. de Gennes, Comm. Energie At. (France) Rappt. No. **925** (1959).
[63] P. Santini, R. Lémanski, and P. Erdös, Adv. Phys. **48**, 537 (1999).
[64] P. Erdös and J. Robinson, *The Physics of Actinide Compounds* (Plenum Press, New York, London, 1983).
[65] J. Neuenschwander, O. Vogt, E. Voit, and P. Wachter, Physica B **144**, 66 (1986).
[66] G.H. Lander, W.G. Stirling, J.M. Rossat-Mignod, M. Hagen, and O. Vogt, Physica B **156 & 157**, 826 (1989).
[67] G.H. Lander, W.G. Stirling, J.M. Rossat-Mignod, J.M. Hagen, and O. Vogt, Phys. Rev. B **41**, 6899 (1990).
[68] W. J. L. Buyers and T. M. Holden, *Neutron Scattering from Spins and Phonons in Actinide Systems*, Handbook on the Physics and Chemistry of the Actinides Vol. 2, edited by A. J. Freeman and G. H. Lander (North-Holland, New York, 1985).
[69] P. de V. DuPlessis, J. Magn. Magn. Mater. **54-57**, 537 (1986).
[70] T.M. Holden, W.J.L. Buyers, P. de V. DuPlessis, K.M. Hughes, and M.F. Collins, J. Magn. Magn. Mater. **54-57**, 1175 (1986).
[71] K.M. Hughes, T.M. Holden, W.J.L. Buyers, P. de V. DuPlessis, and M.F. Collins, J. Appl. Phys. **61**, 3412 (1987).
[72] W. Heisenberg, Z. Phys. **49**, 619 (1928).
[73] F. Bloch, Z. Phys. **57**, 545 (1929).